FAILURE MECHANISM OF GRANULAR SOIL SLOPES UNDER HIGH INTENSITY RAINFALLS

Rong-Her Chen [1], Kwo-Jane Kuo [2], and Wei-Nan Chien [3]

ABSTRACT

This study uses laboratory experiment to clarify the failure mechanism of granular soil slopes when subjected to high rainfall intensity. A rainfall simulator was employed to perform tests on slopes with convex and concave profiles; the slopes were non-homogeneous and had a dip stratum underneath. In addition, different fines contents (0 ~ 12%) and rainfall intensities (78 and 287 mm/hr) were considered as variables. During the experiment, the variations in pore water pressure and volumetric water content in the soil were measured. The characteristics of the failure mechanism and the responses of pore water pressure and water content in the model slopes are compared and discussed as functions of the variables. For samples with fines content of 12%, failure was more likely initiated by surface erosion. In contrast, for samples with fines content less than 10%, slope failures were initiated near the toe, where the soil was highly saturated. The profiles of total head above the impervious stratum were generally nonlinear and the pressure head near the toe of the slope could be even higher than the equivalent head of overburden pressure. Moreover, the initial failure in concave slopes occurred sooner than that in convex slopes; it was attributed to the thin soil layer near the toe of the slope, so that a high hydraulic gradient was induced to cause piping to be initiated. With regard to rainfall intensity (78 versus 287 mm/hr), less time to failure and longer failure surface were observed in the higher intensity condition; however, the length of failure surface and the runout distance were about the same irrespective of slope profiles.

Key words: Model test, slope, granular soil, failure, rainfalls.

1. INTRODUCTION

In recent years, dramatic weather changes due to global warming have resulted in more frequent and severe slope failures, and in Taiwan there have been several recent incidents. On July 17 ~ 19, 2008, Typhoon Kalmaegi brought 1040 mm of rainfall in 48 hours, with the maximum intensity of 148 mm/hr, causing serious flooding in the central and southern parts of Taiwan. Then on August 6 ~ 10, 2009, Typhoon Morakat brought 1400 mm of rainfall in just one day, with a near record-breaking rainfall of 2300 mm in 48 hours and maximum intensity of 117 mm/hr. Again, the southern part of Taiwan was not only inundated by floods in many areas, but a huge landslide was also induced at Shiaoling Village, where hundreds of people were buried by the debris. It is clear that the high intensity and the high amount of rainfall were the predominant factors to cause this disaster. In addition, it is expected that the effects of global warming will increase, resulting in more disasters in the future.

The landslide at Shiaoling was about 1200 m long, 40 m deep, and 2.4 × 10^6 m^3 in volume. The slipped material was mainly composed of pervious colluviums deposited on the top of impervious shale layers, which dip at 15 ~ 25° with the horizontal. Because of the hydraulic characteristics of the geological materials, the high intensity and long duration rainfall allowed water to infiltrate easily and deeply into the slope and to accumulate on top of the impervious strata. As the pore-water pressure within the slope continued to increase, the shear strength of the material gradually decreased until the slope failure was induced.

Many researchers have studied slope failures caused by rainfall infiltration (Lumb 1975; Brand 1982; Iverson and Major 1986; Chen *et al*. 1999; Kim *et al*. 2004; Chen *et al*. 2004; Chen *et al*. 2009). There are also related research topics such as: Rainfall intensity, water supply type (*i.e.*, rainfall or ground water), fines content and/or relative density of soil, and the size of physical model (Wang and Sassa 2003; Chen *et al*. 2004; Moriwaki *et al*. 2004; Orense *et al*. 2004; Tohari *et al*. 2007; Huang *et al*. 2008, *etc*). Furthermore, Ried and Iverson (1992) employed numerical analysis to show that slope profile and hydraulic conductivity of soil are the two dominant factors for slope stability. Regarding slope profile, Lee (1982) reported that slope failures induced by rainfall in Japan were commonly in concave shape.

This current study uses a laboratory experiment to clarify the failure mechanism of granular soil slopes when subjected to high rainfall intensity. A rainfall simulator was employed in the laboratory to perform tests on the slopes with convex and concave profiles. In addition, the tested slopes had a dip stratum underneath because slope failures occur faster in non-homogenous slopes with a dip stratum than in homogeneous slopes (Chen *et al*. 2011). Therefore, non-homogenous slopes are more critical for this study.

2. MODEL TEST

In studying slope failure induced by rainfall infiltration, three commonly adopted methods are site investigation, numerical analysis, and model test. Generally speaking, site investigation is suitable to only case studies and is costly, while the nu-

Manuscript received October 6, 2011; revised February 2, 2012; accepted March 7, 2012.

[1] Professor, Department of Civil Engineering, National Taiwan University, Taipei, Taiwan.

[2] Ph.D. student (corresponding author), Department of Civil Engineering, National Taiwan University, Taipei, Taiwan (email: clay.kuo@ msa.hinet.net)

[3] Former master student, National Taiwan University, Taipei, Taiwan.

merical method needs to collect many parameters related to geological materials. In these respects, model testing is a comparatively efficient method because it can be performed in well controlled conditions such as boundary and loading conditions. More importantly, a test can simulate how slope failure is initiated and it also allows the whole process of failure be observed in the laboratory. Over the past ten years, model tests have been employed by several researchers (Wang and Sassa 2003; Moriwaki *et al*. 2004; Orense *et al*. 2004; Tohari *et al*. 2007; Huang *et al*. 2008).

2.1 Similarity Analysis

When performing a model test, the model and the prototype should be related by satisfying geometric similarity, kinematic similarity, and dynamic similarity to ensure the feasibility and reliability of test results. For instance, the scaling factor of length between the prototype and the model may be chosen as λ (= L_p / L_m) and the materials used in the prototype-slope and the model-slope can be the same, *e.g.*, having the same unit weight. From similarity analysis (Rocha 1957; Roscoe 1968), the relationship between the physical quantities of prototype- and model-slopes is shown in Table 1. Note that λ and ρ are scaling factors. In this study, the value of ρ was equal to 1 and λ was assumed to be 10.

2.2 Experiment Setup

The test device consists of a sand tank supported by a steel frame, with the walls made of 10 mm thick tempered glass. The sand tank is shown in Fig. 1. The experimental setups for convex and concave slopes are shown in Figs. 2(a) and 2(b), respectively. The convex slope has a 20° upper slope and a 30° lower slope; while the slope angles of concave slope are reverse. Both slopes have an impervious stratum inclining at 10° with the horizontal. The flow chute is 0.3 m wide, and the deposition area is 0.6 m wide (Fig. 2(c)).

A rainfall system was set at 1.6 m above the slope to generate uniformly distributed rainfall. The sprinkler system can produce rain drops of less than 0.1 mm in diameter to prevent soil from being eroded by large rain drops. Water can also be supplied from the bottom of the tank to simulate the rise of ground water level, if needed. The rainfall intensities for this study were 78 mm/hr and 287 mm/hr. The low intensity was based on the result of previous studies (Brand 1984; Lumb 1975) that the threshold value for most slopes in Hong Kong to fail was about 70 mm/hr; while the high intensity was to simulate extreme weather conditions.

Pore-water pressures were recorded by piezometers installed close to the impervious stratum, where the variation in pore water pressure was expected to be more significant. The accuracy of the piezometers, Kyowa PGM-G, is ±0.5% and the allowable pressure is 20 kPa. Several moisture sensors, Delta-T SM200, were used to measure the volumetric water content of the soil. The accuracy of the sensor is ±3%, with an operating range between 0 ~ 60°C. Moisture sensors M1-M7 were installed on one side of the tank. The coordinates of the installed sensors and the depths of the piezometers are tabulated in Fig. 2. In addition, three CCD cameras were aimed at different angles, *i.e.*, normal to the side of the tank, the lower slope, and the deposition area to record the process of the test. These cameras have a resolution of 640 × 480 pixels and a maximum frame rate of 30 fps.

2.3 Test Material

The coarse material used for testing is uniform, sub-angular sand with diameter of 0.1 ~ 0.4 mm. It is classified as poorly-graded sand (*SP*) as per the Unified Soil Classification System, with a coefficient of uniformity of C_u = 1.29, a coefficient of curvature of C_c = 0.97, maximum dry unit weight $\gamma_{d,\max}$ = 16.1 kN/m^3, and minimum dry unit weight $\gamma_{d,\min}$ = 13.3 kN/m^3. The fine material used for testing was quartz powder with diameter in the range of 0.001 ~ 0.1 mm and is classified as silty fine sand (*ML*). The grain size distribution curves of the test sand and the fines are shown in Fig. 3.

There were four kinds of sample tested, each with different fines content. For example, sample S0 was composed of 100% sand and no fines; sample S5 was a mixture of 5% fines and 95% sand, and so on. Table 2 shows the test program and soil properties. In the test program, the symbols V, C, H, and L represent convex, concave, high rainfall intensity, and low rainfall intensity, respectively. The saturated volumetric water content of soil is obtained from the soil-water characteristics curve using pressure plate test. The friction angles of the sand are obtained by triaxial consolidated-undrained test at relative densities of 55% and confining pressures of 50, 100, and 200 kPa, respectively. The friction angles of samples S0 and S10 are 36.6° and 35.1°, respectively.

When conducting model tests, strictly speaking, the rainfall intensity and the hydraulic conductivity of the soil should be modified. However, the hydraulic conductivity of the soil was so small that the modified value seems to have had little effect on test results. Furthermore, the scaling factors for the two quantities are the same, and so the rainfall intensity was not modified.

2.4 Test Procedure

The test procedures are briefly described as follows.

1. The inclined impervious stratum, made of plywood, was placed at the beginning. Then the gap between this stratum and the wall of the tank was sealed with silicone sealant to make it waterproof.

Table 1 Dimensional analysis of the physical quantities in model testing (modified from Chen and Chi 2010)

Physical quantity	Relationship
Length	$L_m = (1/\lambda)\, L_p$
Slope angle	$\theta_m = \theta_p$
Unit weight	$\gamma_m = (1/\rho)\, \gamma_p = \gamma_p$
Friction angle	$\phi_m = \phi_p$
Pore water pressure (or stress)	$u_m = (1/\lambda)\, u_p$
Strain	$\varepsilon_m = \varepsilon_p$
Time	$t_m = (1/\sqrt{\lambda})\, t_p$

Remark: λ and ρ are scaling factors

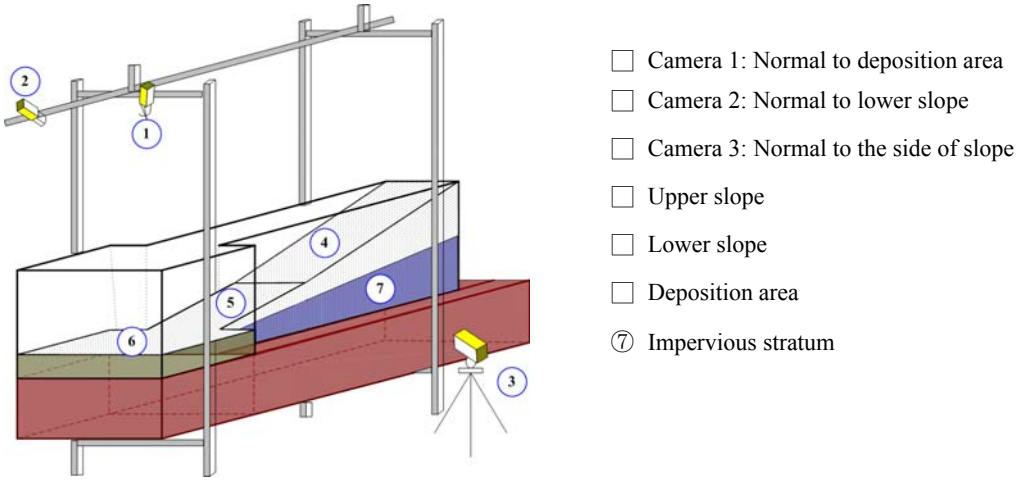

Fig. 1 Test sand tank

Piezometer	Coordinate (X, Y)	Depth (m)
P1	(0.95, 0.29)	0.261
P2	(0.60, 0.24)	0.180
P3	(0.35, 0.19)	0.112
P4	(0.17, 0.15)	0.051

Moisture sensor	Coordinate (X, Y)
M1	(0.94, 0.39)
M2	(0.80, 0.39)
M3	(0.56, 0.34)
M4	(0.52, 0.30)
M5	(0.40, 0.29)
M6	(0.24, 0.20)
M7	(0.11, 0.13)

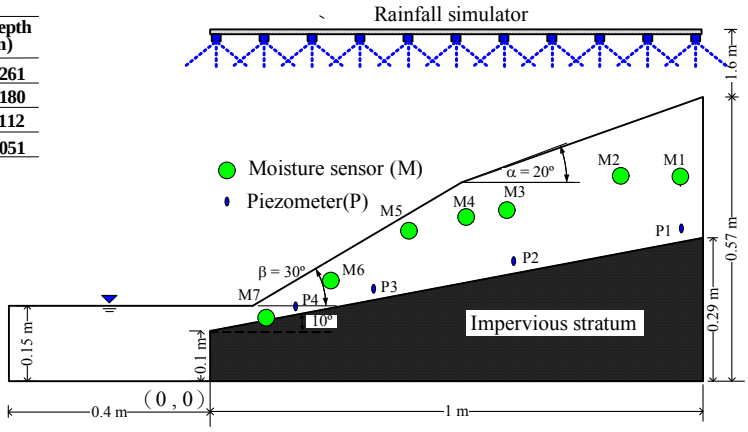

(a) Side view of convex slope

Moisture sensor	Coordinate (X, Y)
M1	(0.94, 0.39)
M2	(0.80, 0.39)
M3	(0.56, 0.27)
M4	(0.52, 0.25)
M5	(0.40, 0.23)
M6	(0.24, 0.16)
M7	(0.11, 0.13)

Piezometer	Depth (m)
P1	0.251
P2	0.096
P3	0.039
P4	0.016

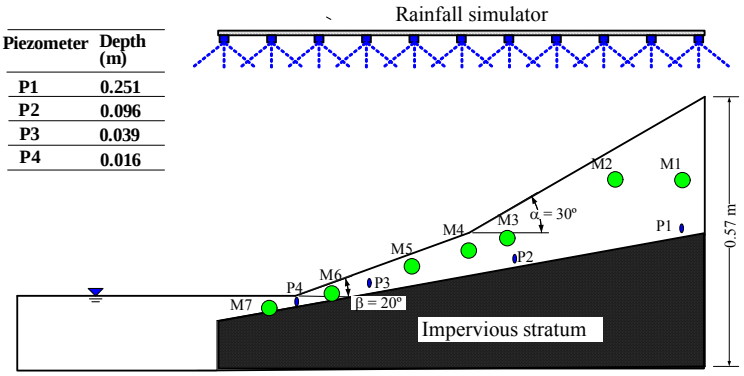

(b) Side view of concave slope

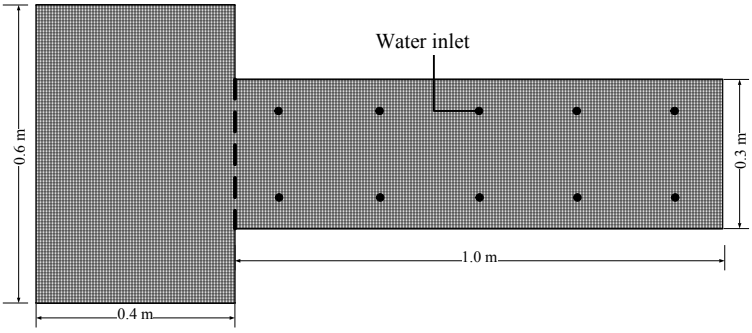

(c) Top view of sand tank

Fig. 2 Experimental setup: (a) Side view of convex slope; (b) Side view of concave slope; (c) Top view of sand tank

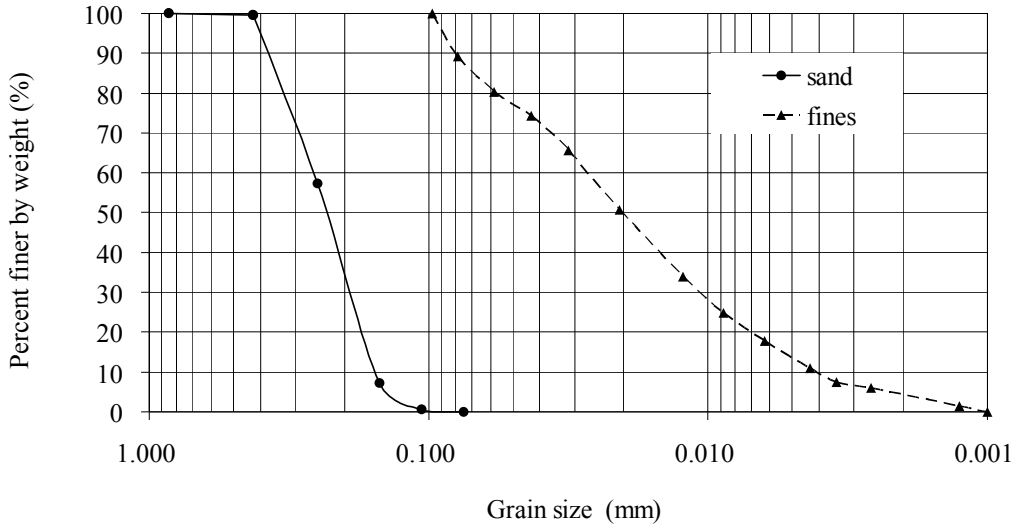

Fig. 3 Grain size distribution curves of the test sand and fines

Table 2 Test program and soil parameters

Test	Profile	Sample	Fines Content %	β deg.	α deg.	I mm/hr	γ_d kN/m^3	γ_{sat} kN/m^3	θ_s %	k_s ($\times 10^{-4}$) m/s	ϕ deg.
V0H	Convex	S0	0	30	20	287	14.7	19.0	45.0	1.43	36.6
V0L		S0	0	30	20	78	14.7	19.0	45.0	1.43	36.6
V5L		S5	5	30	20	78	15.1	19.3	42.0	0.26	–
V10L		S10	10	30	20	78	15.3	19.4	41.5	0.13	35.1
C0H	Concave	S0	0	20	30	287	14.7	19.0	45.0	1.43	36.6
C0L		S0	0	20	30	78	14.7	19.0	45.0	1.43	36.6
C5L		S5	5	20	30	78	15.1	19.3	42.0	0.26	–
C10L		S10	10	20	30	78	15.3	19.4	41.5	0.13	35.1
C12H		S12	12	20	30	287	15.5	19.5	40.8	0.068	–

Remark: α = upper slope angle, β = lower slope angle, I = rainfall intensity, γ_d = dry unit weight, γ_{sat} = saturated unit weight, θ_s = saturated volumetric water content, k_s = saturated coefficient of hydraulic conductivity, ϕ = friction angle

2. The slope was then formed, with the help of a shaping plate to retain soil in place. Subsequently, the soil was pluviated in layers, each being 0.025 m thick, from the bottom to the top. In addition, the plate was lifted after each layer of soil had been placed. This procedure was repeated till a specified full height was reached. With this method, the relative density of the sample should be approximately 55%.
3. The water valve at the bottom of the tank was opened to allow water to flow slowly into the tank. After the water table had reached the top of the slope, the valve was closed. The slope was then left 12 hours for soaking in order to reach as much saturation as possible.
4. Later, the valve was reopened to let water drain out until the water table was lowered to the elevation at the toe of the slope. It usually took about several hours for the water to drain, a rate of 5×10^{-4} m^3/min, so that the settlement of soil was insignificant.
5. The monitoring system was turned on, including CCDs, moisture sensors, and piezometers.
6. The infiltration test was started by turning on the sprinkler system to generate rainfall with a specified intensity.
7. When there was no significant movement of soil observed, the test was terminated.

Note that the purpose of soaking soil before testing was not only to simulate the effect of precedent rainfall in the field but also to expedite the test.

3. TEST RESULTS

The following test results describe the observed failure process, the variations in volumetric water content and pore-water pressure in the soil. The characteristics of the failure mechanism as well as the responses of pore water pressure and water content in the model slopes of various slope profiles, fines contents, and rainfall conditions are discussed.

3.1 Failure Process

The observations showed that slope failure was initiated as piping occurred at the toe of the slope, after which, the failure extended upward and induced retrogressive shallow slides. The phenomena in which the fines were flowing out of the slopes are shown in Fig. 4. In Test-V5L, the flow was small in quantity, low concentration, and light color. By contrast, the flow in Test-V10L was faster and had more quantity. Later, erosion by water flow continuously progressed into the slope and caused gradual collapses of soil. According to previous research (Thevanayagam, 1998), fine materials will flow through and out of the interstices of coarse material if the ratio between two materials' medium diameters, D_{50} / d_{50}, is greater than 6.5. In this study, the ratio between sand and fines was about 10. Hence, the fines could be washed out, and even piping was induced when the hydraulic gradient was high enough.

Several final surfaces are depicted for comparison. Herein, the final surface is defined at time t_e (Table 3) when mass movement was insignificant. In Fig. 5(a), Test-V0L had only shallow flow failure occurring at the toe of the slope. On the other hand, the failure surface of Test-V5L extended to about the middle of the lower slope, while the failure surface of Test-V10L extended even upwards and was also deeper. Thus, larger failure surfaces occurred in soils with more fines, and this result was observed irrespective of the slope profiles (Figs. 5(a) and 5(b)). Furthermore, comparing V10L and C10L, the convex slope had deeper failure surface and thicker deposition area than the concave slope.

As to the effect of high rainfall intensity, the induced failure surface was, as expected, deeper and the deposition was longer than under lower rainfall intensities; furthermore, the convex slope had a deposit angle of 11° and the concave slope had a gentler angle of 8°. It is also shown in Table 3 that the failure lengths of V0H and C0H were about the same (570 mm versus 578 mm). Herein, the failure length is defined as the length of failure surface, measured from the toe of the slope to the upper end of the surface. This result was unlike those with low rainfall intensities.

The failure length and the time to the end of failure also varied with fines content and rainfall intensity. In Fig. 6, the soil with more fines failed earlier and the corresponding failure surface developed faster and longer. The reason could be due to the samples with more fines content having lower friction angle and higher unit weight (Table 2). In Fig. 7, it can be seen the solid curves for high rainfall intensity are steeper than the dotted curves for low intensity. In other words, less failure time and longer failure length were observed under higher intensity condition. This figure also shows concave slopes failed earlier than convex slopes. However, the two solid curves attain about the same failure length as mentioned above. The above observation can be explained from the aspect of the hydraulic gradient near the toe of a slope. Further details are discussed in the section of pore-pressure.

The variation of slope surface condition for concave slopes with different fines content is shown in Fig. 8. For samples with fines content less than 10%, as shown in Figs. 8(a) ~ 8(c), the slope surfaces had insignificant to small rills developed at final stage. It can also be seen that samples S0 and S5 had obvious large scarps after failure, while sample S10 had only small scarps and rills.

Table 3 Summary of test results

Test	S_i %	S_f %	F_l mm	R_l mm	h_{p4} mm	t_p s	t_e s	$t_e - t_p$ s
V0H	49.7	97.9	570	400	52	320	4200	3880
V0L	60.1	77.4	150	110	37	1056	3960	2904
V5L	55.4	82.5	255	166	49	645	3200	2555
V10L	53.6	88.9	432	213	48	210	4365	4155
C0H	–	–	578	444	41	36	1905	1869
C0L	–	–	375	283	10	759	3000	2241
C5L	–	–	458	285	43	540	4500	3960
C10L	–	–	473	296	1	162	1320	1158
C12H	–	–	–	–	–	39690	–	–

Remark: S_i = initial degree of saturation measured at M2, S_f = final degree of saturation measured at M2, F_l = failure length measured from the toe of the slope to the end of failure surface, R_l = runout distance, h_{p4} = pressure head of P4 measured at t_p, t_p = time when initial piping was observed, t_e = the time at the end of significant mass movement, $t_e - t_p$ = duration of failure process

For the sample containing 12% fines, settlement was induced both during soaking the slope and after draining the water out of the sand tank. Besides, a different failure mechanism was observed. Because only a small amount of rainwater could infiltrate into the slope, no significant changes in water content and pore-pressure were measured. In this soil, the failure process can be distinguished into three different stages (Fig. 8(d)). At the initial stage, there was obvious runoff flowing on the loose surface of slope, so the soil was quickly carried away and deposited at the toe of the slope. After three hours of rainfall, several small irregular rills had gradually developed on the upper slope, with small parallel rills appearing on the lower slope. Seven hours later, the small rills had merged into large gullies. Subsequently, as more runoff flowed on the lower slope, the gullies gradually deepened until about eleven hours, when piping was noticed at the toe of the slope.

3.2 Volumetric Water Content

A typical example showing the variations in volumetric water content and pore water pressure during testing is presented in Fig. 9(a). Two moisture sensors and one piezometer are chosen for explanation. At the beginning of the test, sensor M7 near the toe of the slope had a high initial degree of saturation, about 95%, due to the preceding soaking of the sample. However, sensor M2, located at the upper part of the slope, had only 50% of initial degree of saturation, and so more obvious changes in water content at M2 could be measured. Likewise, piezometer P4, located near the toe, had also noticeable changes in pore water pressure.

The curves shown in Fig. 9(a) were obtained from Test-V0H. These curves may be divided into following three stages separated by t_p and t_f. The definition of t_p is the time when initial failure occurred and when piping was observed, while t_f is the time when obvious mass movement was initiated. Note that the curve of M2 has obvious inflection points at t_p and t_f, and the curve of P4 is hyperbolic shape. By contrast, the volumetric water content at M7 varied only slightly, due to the high initial degree of saturation. This suggests that failure was predominantly caused by the increase in pore water pressure rather than soil saturation.

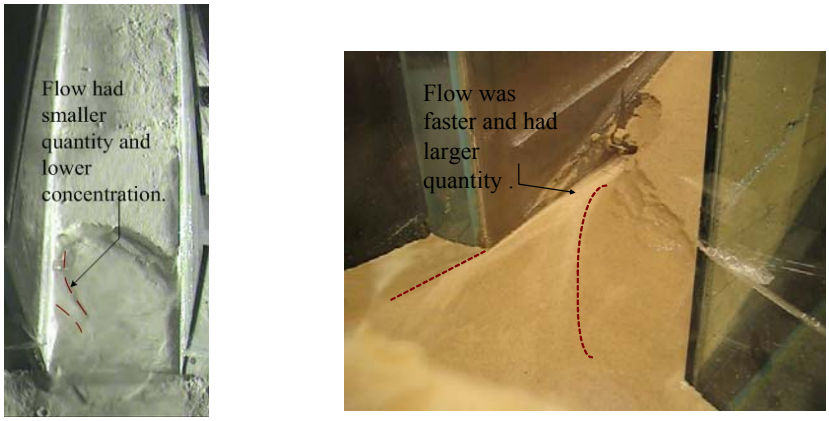

(a) Test-V5L (b) Test-V10L

Fig. 4 Fines flowing out of convex slopes: (a) Test-V5L; (b) Test-V10L

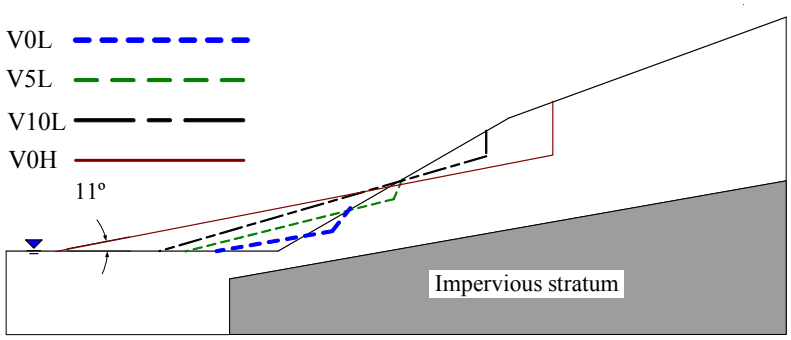

(a) Convex slope

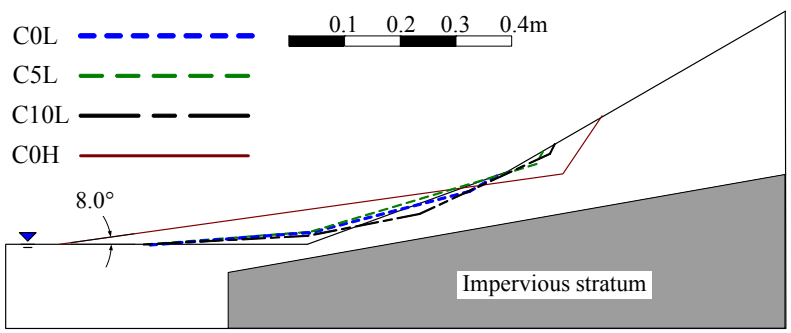

(b) Concave slope

Fig. 5 Final surfaces of the slopes composed of soils with different fines contents: (a) convex slope; (b) concave slope

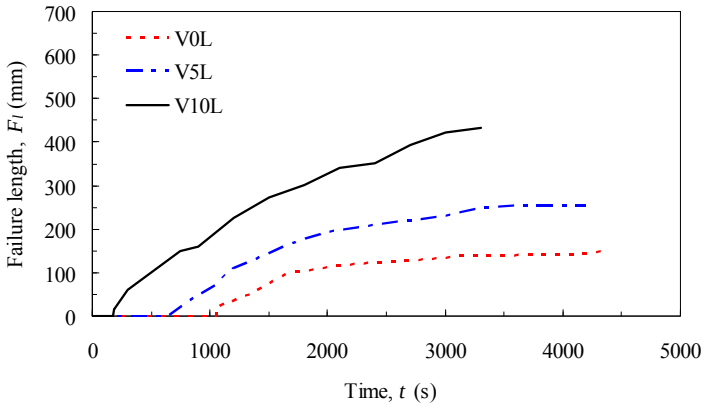

Fig. 6 Failure length versus time for the convex slopes composed of soils with various fines content (I = 78 mm/hr)

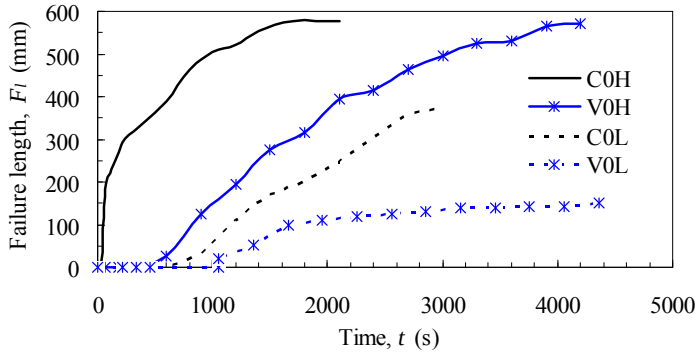

Fig. 7 Comparison of failure length versus time for sand slopes subjected to rainfall of different intensities

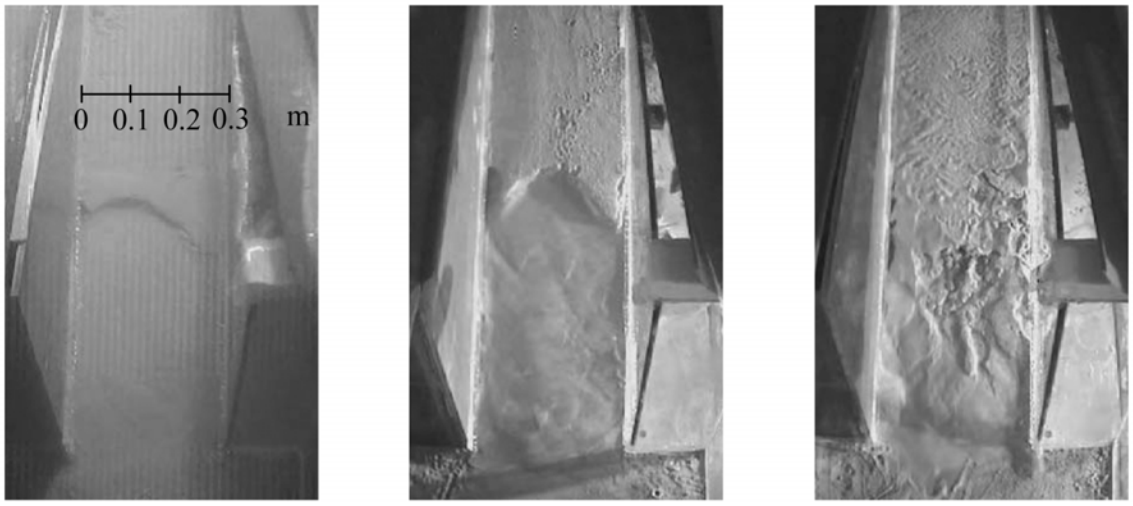

at final stage (a) C0L (Sample S0)

at final stage (b) C5L (Sample S5)

at final stage (c) C10L (Sample S10)

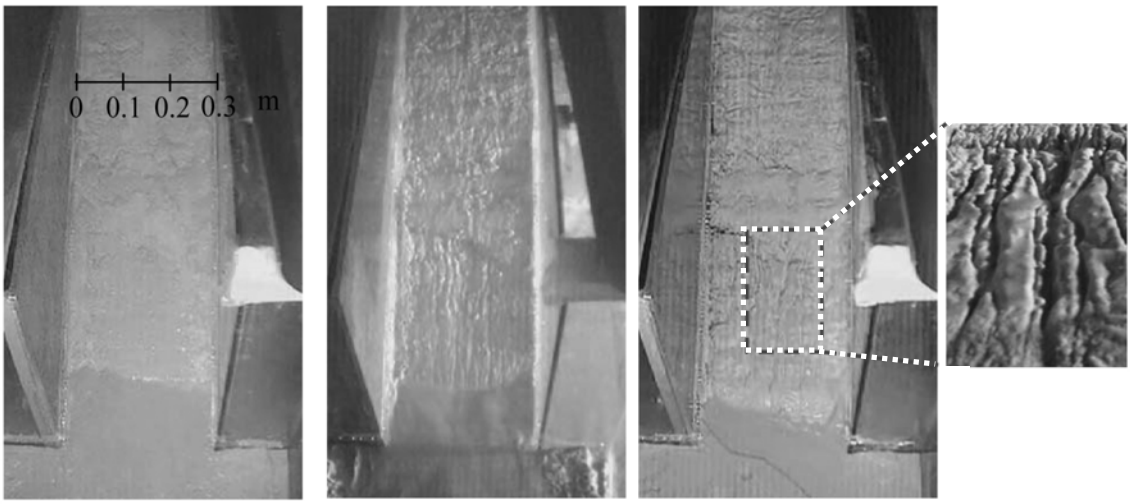

at initial stage 3 hours later 7 hours later

(d) C12L (Sample S12)

Fig. 8 Parallel rills developed in soils of different fines content for concave slopes

1. Initial stage: From the beginning to the occurrence of initial failure when piping was observed. The time t_p was at 320s.
2. Progressive failure stage: From t_p to t_f (= 800s), when an obvious mass movement was initiated. During this stage both the volumetric water content at M2 and the pore water pressure at P4 were increasing rapidly.
3. Final stage: After about 2000s, all the curves became stable. A retrogressive type of failure continued, extending to the intersection between the upper and lower slopes. Then the upper slope started to collapse, forming a vertical scarp on the slope face.

The variation in water content depends also on fines content and rainfall intensity. In Fig. 9(b), the maximum difference in volumetric water content among the three tests (V0L, V5L, and V10L) was not more than 5%, and the variation gradually became insignificant as time went on. It can also be seen that high rainfall intensity induced both higher rate of change and higher volumetric water content than induced by lower rainfall intensities.

3.3 Pore Water Pressure

The effect of fines content on pore water pressure variation is demonstrated in Fig. 10, which shows the pressure head measured at P4 (h_{p4}) for three tests with various amounts of fines. As the fines content increased, the pore water pressure built up faster, and so t_p was less. The values of t_p and h_{p4} for each test are tabulated in Table 3. This table also shows the high rainfall intensity resulted in higher h_{p4} and less t_p than the low rainfall intensity did, *e.g.*, V0H versus V0L.

The total head profiles at two different times, t_p and t_e, for convex and concave slopes are shown in Figs. 11 and 12, respectively. The profiles are generally nonlinear and have a high gradient near the toe of the slope. For example, at t_p when piping occurred, the hydraulic gradients near the toes of both slopes (Figs. 11(a) and 12(a)) were higher than those of the other piezometers. Furthermore, the total head at the toe was close to the surface for the convex slope (Fig. 11(a)); it was even higher for the concave slope (Fig. 12(a)).

For the sake of comparison, the hydraulic gradient at t_p for each test is tabulated in Table 4. As shown in the table, the hydraulic gradients of concave slopes were generally higher than those of convex slopes. This suggests, *e.g.*, C0H (i_{34} = 0.41) would fail earlier than V0H (i_{34} = 0.23), and vice versa. At t_e when significant mass movement ended, the total head profiles (Figs. 11(b) and 12(b)) were higher than the profiles at time t_p, which can be attributed to continuous accumulation of pore water pressure. Thus, the higher hydraulic gradient, resulting in larger seepage force and less shear strength of soil, in the concave slope could induce longer failure length than the convex slope, even though the former was gentler than the latter (20° versus 30°).

Moriwaki *et al.* (2004) conducted a full-scale experiment to clarify the failure process of a landslide triggered by rainfall. The soil was loose sand with relative density of 35% and initial water content of 8%. A similar result, in which the pressure head at the toe of the slope was higher than the head equivalent to overburden pressure, was also measured. They concluded this resulted from the compression of soil mass.

For convex slopes, the profiles at t_e were higher for higher fines content and rainfall intensity (Fig. 11(b)), though the profiles at t_p were not significantly different (Fig. 11(a)). In addition, the differences for concave slopes are less significant (Fig. 12).

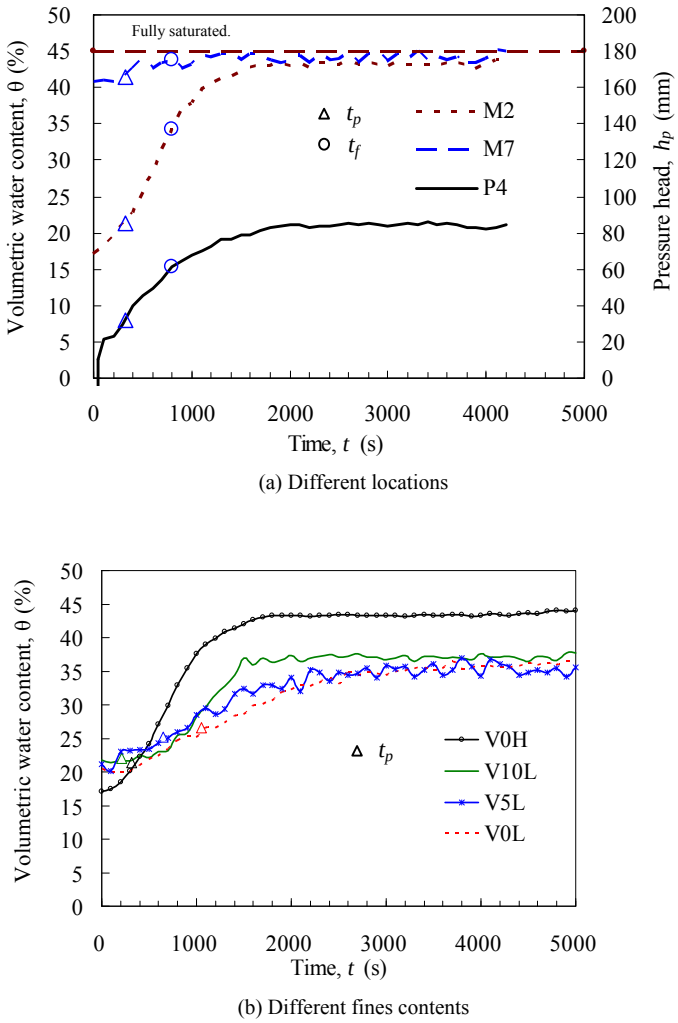

Fig. 9 Variations of volumetric water content and pressure head: (a) different locations (Test-V0H); (b) different fines contents (moisture sensor M1)

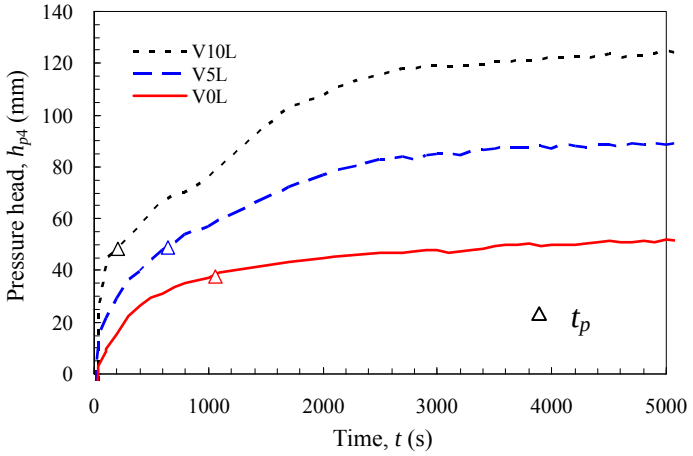

Fig. 10 Variations of pressure head in the convex slopes consisted of soils with different fines contents (P4, I = 78 mm/hr)

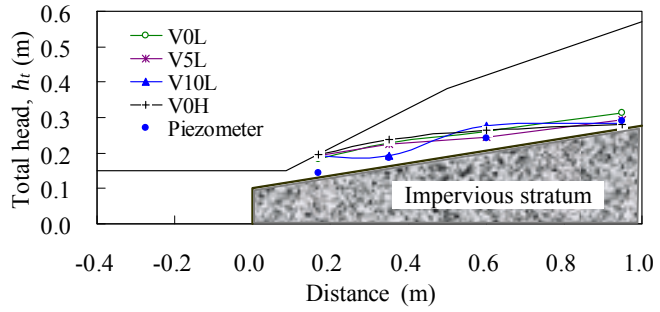

(a) At time t_p

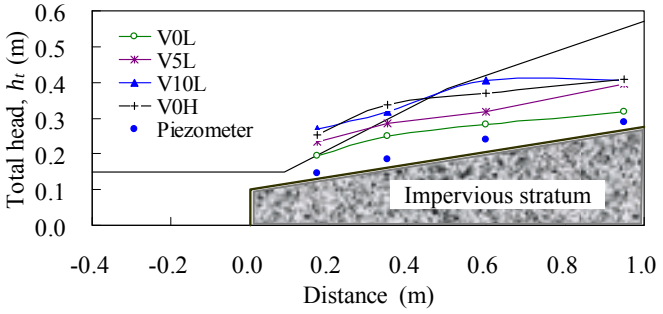

(b) At time t_e

Fig. 11 Total head profiles in a convex slope: (a) at time t_p; (b) at time t_e

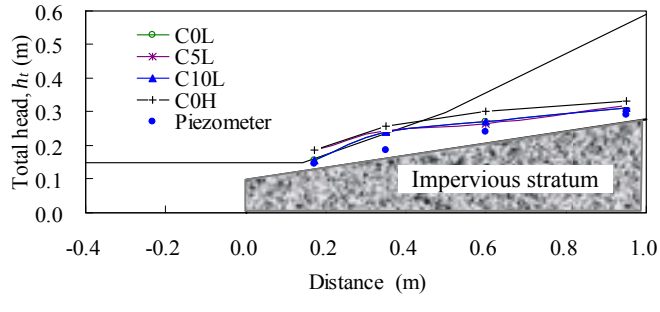

(a) At time t_p

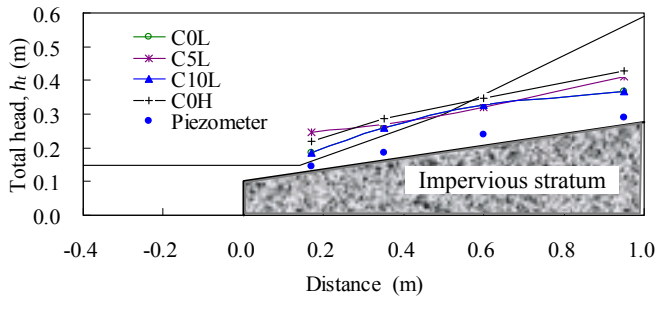

(b) At time t_e

Fig. 12 Total head profiles in a concave slope: (a) at time t_p; (b) at time t_e

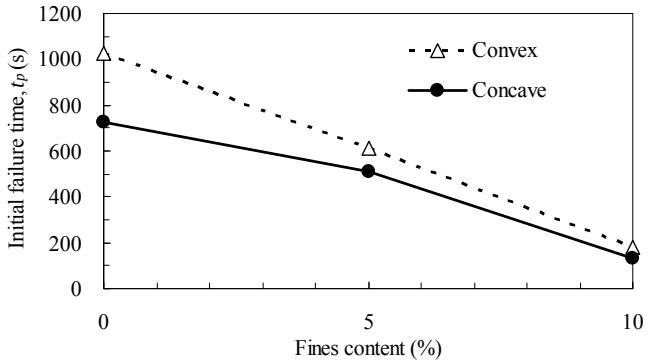

Fig. 13 Initial failure time for convex and concave slopes composed of soils with different fines contents (I = 78 mm/hr)

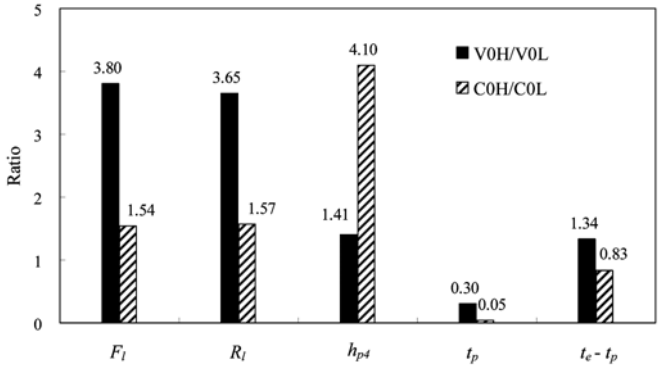

Fig. 14 Ratios of several parameters under high and low rainfall intensities (Sample S0)

Table 4 Total head and hydraulic gradient at time t_p for each test

Test	Total head (mm)				Hydraulic gradient		
	h_1	h_2	h_3	h_4	i_{12}	i_{23}	i_{34}
V0H	282	264	238	196	0.05	0.10	0.23
V0L	313	260	229	182	0.15	0.12	0.26
V5L	293	243	225	194	0.14	0.07	0.17
V10L	–	–	–	–	–	–	–
C0H	332	302	259	186	0.09	0.17	0.41
C0L	313	271	241	155	0.12	0.12	0.48
C5L	317	264	244	188	0.15	0.08	0.31
C10L	310	255	220	146	0.16	0.14	0.41
C12H	–	–	–	–	–	–	–

Remark: h_1 = total head of P1 measured at t_p
i_{12} = hydraulic gradient between P1 and P2

4. DISCUSSION

The effect of fines content on failure initiation is shown in Fig. 13, in which t_p decreases with increasing fines content of the sample. It is also apparent that concave slopes took less time to initiate failures than convex slopes, though this difference gradually became insignificant as the fines content increased.

In order to focus on the effect of rainfall intensity (78 versus 287 mm/hr), several parameters are considered as follows: Failure length, F_l; runout distance, R_l; the pressure head at P4 when piping occurred, h_{p4}; the time of piping, t_p; and the duration of failure process, t_e - t_p. These parameters are compared by the ratio of the values obtained under high and low rainfall intensities, respectively. The soil for comparison is sample S0. These values are tabulated in Table 3.

In Fig. 14, the solid bars stand for the ratios of convex slopes, V0H/V0L, while the slash bars stand for those of concave slopes, C0H/C0L. For the first two parameters, F_l and R_l, the ratios for convex slopes are 3.80 and 3.65, and for concave slopes are 1.54 and 1.57, respectively. In other words, the ratios of F_l and R_l are about the same irrespective of the slope profiles. This may be because the quantity of soil removed from the slope was about the same as the quantity of soil deposited at the toe of the slope. It is also note worthy that these ratios, 3.80 and 3.65, approximate the ratio of rainfall intensity, 3.7 (= 287/78). By contrast, the ratios for concave slopes are only 1.54 and 1.57, probably due to inadequate amounts of soil available for removal by the rainfall. This result also implies that the rainfall would have caused as much soil to fail as it could if there was enough soil.

With regard to h_{p4}, the trend is reverse; *i.e.*, the ratio for concave slope is 4.10 and for convex slope is 1.41. This result is not surprising because the soil at P4 was so thin that water could not pass through easily. As a result, the pore water pressure accumulated and rose up easily when the slope was subjected to high rainfall intensity. Consequently, initial failure occurred sooner for concave slopes than for convex slopes, as illustrated by the ratios of t_p, 0.05 and 0.30, respectively.

The duration of failure process can be represented by the time interval between t_p and t_e, *i.e.*, t_e - t_p. Estimated from Table 3, the ratios of duration for convex and concave slopes are 1.34 and 0.83, respectively. This result is apparently connected to the slope profile that determined the removable soil, which in turn depended on the shear strength of the soil. Since the convex slope was thicker than the concave slope, the ratio for the convex slope is thus higher than that for the concave slope.

5. CONCLUSIONS

This experiment employed a rainfall simulator to generate rainfall on model slopes of different profiles to study slope stabilities. The slopes were composed of sandy soils with a variety of fines contents and had a dip stratum at the bottom. The characteristics of the failure mechanism and the responses in pore water pressure and water contents were observed.

For samples with fines content less than 10%, slope failures were initiated close to the toe, where the soil had high degree of saturation. Initial failure was noticed as piping occurred at the toe of the slope. As water continued to infiltrate into the slope, the saturated zone propagated upwards. Meanwhile, the pore water pressure accumulated and raised high enough to cause a series of retrogressive failures. In general, concave slopes failed earlier than convex slopes. This can be attributed to the thin soil near the toe of the slope, so that a high hydraulic gradient was induced, which caused the piping to be initiated. In contrast, the slope with high fines content of 12% showed a different failure mechanism, in which failure was more likely initiated by surface erosion.

Under low rainfall intensity, the soils with more fines induced higher degree of saturation than those with lower fines content. When subjected to high rainfall intensity, the soil was near fully saturated in the vicinity of failure zone, where the degree of saturation could be as much as 90%. It is also note worthy that the curve of volumetric water content versus time has two inflection points at t_p and t_f; the steepest section between the two inflection points indicates the failure process was on going.

The profiles of total head above the impervious stratum were generally nonlinear because the dynamic pore water pressure varied with time. Usually the hydraulic gradient was higher near the toe than any other places in the slope. The pressure head near the toe of the slope could be even higher than the equivalent head of overburden pressure. Moreover, the hydraulic gradients in concave slopes were generally higher than those of convex slopes. Thus, the higher hydraulic gradient in the concave slope could induce longer failure length than the convex slope, even though the former was gentler than the latter. It was also found that fines content affected the failure mechanism, the dimension of failure surface, and the time when piping occurred.

Regarding the rainfall intensity, it significantly affected the scale of failure mass. If there was enough available soil, high rainfall intensity would quickly remove as much soil as possible. This was illustrated by the ratios of F_l and R_l under high and low rainfall intensities, respectively, being about the same irrespective of slope profiles. In other words, the amount of soil that can be removed is proportional to the rainfall intensity. This explains why the recent catastrophes induced by typhoons Kalmaegi and Morakat were so devastating.

This study shows that different types of remedial work may be applied to stabilize slopes, depending on soil properties. For soils with fines content less than 10%, work to prevent piping is especially important in the vicinity of the toe of the slope, either enhancing drainage or reinforcing the toe zone. On the contrary, for soil with high fines content, since failure was more likely initiated by surface erosion, anti-erosion works applied to the slope surface will be more effective.

ACKNOWLEDGEMENTS

This research was financially supported by the National Science Council, ROC, Project Nos. NSC 96-2627-M-002-008 and NSC 97-2627-M-002-005.

REFERENCES

Brand, E. W. (1982). "Analysis and design in residual soil." *Proceedings of the ASCE Geotechnical Engineering Division, Specialty Conference – Engineering and Construction in Tropical and Residual Soils*, Honolulu, Hawaii, 89–141.

Chen H., Chen, R. H., and Lin, M. L. (1999). "Initiation of the Tungmen debris flow, eastern Taiwan." *Environmental and Engineering Geosciences*, **5**(4), 459–473.

Chen, H., Chen, R. H., Yu, F. C., Chen, W. S., and Hung, J. J. (2004). "The Inspection of the triggering mechanism for a hazardous

mudflow in an urbanized territory." *Environmental Geology*, **45**(7), 899–906.

Chen, R. H., Chen, H. P., and Chen, K. S. (2009). "Simulation of a slope failure induced by rainfall infiltration." *Environmental Geology*, **58**(5), 943–952.

Chen, R. H. and Chi, P. C. (2010). "Dimension analysis of model tests on slopes." *Sino-Geotechnics*, **125**, 7–14 (in Chinese).

Chen, R. H., Kuo, K. J., and Chang, C. M. (2011). "Experiment on the stability of granular soil slopes by rainfall infiltration." *5th International Conference on Debris-Flow Hazards Mitigation, Mechanics, Prediction and Assessment*, Padua, Italy, 303–311.

Huang, C. C., Lo, C. L., Jang, J. S., and Hwu, L. K. (2008). "Internal soil moisture response to rainfall-induced slope failures and debris discharge." *Engineering Geology*, **101**(3), 134–145.

Iverson, R. M. and Major, J. J. (1986). "Ground water seepage vectors and the potential for hillslope failure and debris flow mobilization." *Water Resources Research*, **22**(11), 1543–1548.

Kim, J., Jeong, S., Park, S., and Sharma, J. (2004). "Influence of rainfall-induced wetting on the stability of slopes in weathered soils." *Engineering Geology*, **75**(3), 251–262.

Lee, S. W. (1982). "Slope land failure in Japan." *Modern Construction*, **3**, 97-106 (in Chinese).

Lumb, P. (1975). "Slope failure in Hong Kong." *Quarterly Journal of Engineering Geology*, **8**, 31–65.

Moriwaki, H., Inokuchi, T., Hattanji, T., Sassa, K., Ochiai, H., and Wang, G. (2004). "Failure processes in a full-scale landslide experiment using a rainfall simulator." *Landslides*, **1**(4), 277–288.

Orense, R. P., Shimoma, S., Maeda, K., and Towhata, I. (2004). "Instrumented model slope failure due to water seepage." *Journal of Natural Disaster Science*, **26**(1), 15–26.

Reid, M. F. and Iverson, R. M. (1992). "Gravity-driven groundwater flow and slope failure potential 2. Effects of slope morphology, material properties, and hydraulic heterogeneity." *Water Resources Research*, **28**(3), 939–950.

Rocha, M. (1957). "The possibility of solving soil mechanics problems by the use of models." *4th International Conference on Soil Mechanics and Foundation Engineering,* London, U.K., **1**, 183–188.

Roscoe, K. (1968). "Soils and model tests." *Journal of Strain Analysis*, **3**(1), 57–64.

Thevanayagam, S. (1998). "Role of intergrain contacts, friction, and interactions on undrained response of granular mixes." *Proceedings of the International Workshop on the Physics and Mechanics of Soil Liquefaction*, Baltimore, U.S.A., 67–78.

Tohari, A., Nishigaki, M., and Komatsu, M. (2007). "Laboratory rainfall-induced slope failure with moisture content measurement." *Journal of Geotechnical and Geoenvironmental Engineering*, ASCE, **133**(5), 575–587.

Wang, G. and Sassa, K. (2003). "Pore-water pressure generation and movement of rainfall-induced landslides: Effects of grain size and fine-particle content." *Engineering Geology*, **69**(2), 109–125.